Optimized Basis Functions for Slot Antennas Excited by Coplanar Waveguides

Andrea Neto, *Member, IEEE*, Peter De Maagt, *Senior Member, IEEE*, and Stefano Maci, *Senior Member, IEEE*

***Abstract*—A method is proposed for the analysis of slot antennas excited by coplanar waveguides. First, a standard integral equation for the continuity of the magnetic field is formulated. Then the appropriate equivalent magnetic currents of the method of moments are represented in terms of entire-domain basis functions which synthesize the resonant behavior of the slot and the field in proximity of the feeding source and of the bends. In order to define these basis functions, canonical geometries are identified, whose Green's functions have been found analytically. The accuracy and the effectiveness of the method in terms of convergence rate and number of unknowns is demonstrated by comparison with a standard fine meshing full-wave analysis.**

***Index Terms*—Coplanar waveguides, entire domain basis functions, method of moments, slot antennas, submillimeter wave antennas.**

I. Introduction

In MILLIMETER and submillimeter wavelength applications [1]–[4], slot antennas excited by coplanar waveguides (CPW) have been receiving a lot of attention. They are widely being used as feeds in dielectric lens antennas for single-pixel atmospherical and astronomical instruments. CPWs allow the introduction of lumped elements and can help avoid some technological difficulties related to the manufacturing of microstrips at millimeter wavelengths. However, even though the geometry of these antennas is relatively simple, the accurate characterization of their input impedance for actual feed structures is not a straightforward matter. An accurate solution [5], [6] for these problems is based on a full-wave method of moments (MoM) analysis. Possible network-based simplifications which appear quite reasonable for other feed types [7] do not apply as well to a CPW feed. In [8], it was shown that applying MoM to the radiating slots individually and then connecting their evaluated input impedance to an equivalent transmission line simulating the CPW can lead to inaccuracies in predicting the resonant frequency. Errors up to 5% were observed as the relative dimensions of the slot became larger with respect to the CPW width. A complete full-wave analysis with discretization of both slot and feeding CPW is then unavoidable if one wishes to obtain sufficient accuracy. Unfortunately, a conventional MoM based on small-domain basis functions leads to large matrices which may be ill-conditioned close to the antenna resonant frequency. This results in a high-accuracy needed for the calculation of the MoM coupling integrals. Even if this is not a difficult task for a single or a few slot antennas, it becomes problematic for large-and medium-sized arrays [9]. Such arrays are foreseen to be needed for future space missions. Accordingly, the aim of this paper is the definition of problem-matched basis functions allowing the reduction of the MoM matrix size. In order to clarify the physics involved, this paper will focus on the case of single- and double-slot CPW-fed antennas. However, the major benefit of the method, which is a considerable reduction in computation time, becomes even more appreciable for array applications.

The procedure proposed here to define entire-domain MoM basis functions is based on the Green's functions of the infinite slot-line and of the infinite CPW, etched on a ground plane between two different semi-infinite dielectrics. The solutions of these reference problems have been found in analytical forms [10]–[12], and they provide two kinds of basis functions. The first kind describes the field in the proximity of the delta gap. The second kind describes the CPW wave propagation and slot resonance by interference of two traveling waves; the relevant propagation constants are dictated by the dispersion equation associated to the above infinite reference problems. All the connections through 90° bends are treated by modifications of the previously defined entire-domain basis functions.

The present method allows the reduction of the number of unknowns while preserving the same accuracy of a standard fine meshing full-wave analysis. Moreover, due to the reduced dimension of the MoM matrix, the accuracy needed in the calculation of the various mutual coupling integrals can be relaxed without introducing significant errors in the matrix inversion. Physical insight is also gained, since each one of the basis functions can be associated with a specific electromagnetic mechanism which is essentially regulated by one of the geometrical parameters. This also provides some design guidelines.

The procedure proposed in this paper can also be used as a matrix-compression technique when the basis functions are viewed as ruling the grouping of the subdomain unknowns; this leads to the possibility of applying the present method in the framework of a conventional, subdomain algorithm.

It is also worth noting that the use of infinite open waveguide Green's function problem can be systematically generalized by resorting to the formulation proposed in [13]–[15]. From this general formulation, which in [13]–[15] is used the scope to analyze the leakage effects of open-waveguide leaky antennas, one can deduce basis functions for the full-wave analysis of more general antenna structures.

Manuscript received April 5, 2001; revised May 20, 2002.

A. Neto was with the Sub-mm Wave Advanced Technology Group, Caltech-Jet Propulsion Laboratory, Pasadena, CA 91109 USA. He is now with FEL-TNO, Den Haag 2597 AK, The Netherlands.

P. De Maagt is with the Electromagnetic Division, European Space Research and Technology Center, 2200 AG Noordwijk, The Netherlands (e-mail: peter.de.maagt@esa.int).

S. Maci is with the Department of Information Engineering, University of Siena, 53100, Siena, Italy (e-mail: macis@ing.unisi.it).

Digital Object Identifier 10.1109/TAP.2003.813636

The paper is structured as follows. Section II summarizes the formulation for the continuity of the magnetic field integral equation (CMFIE) applied to a certain number of actual configurations. The formulation for both small-domain and large-domain basis functions is also given in order to view the entire-domain solution in terms of MoM matrix compression. In Section III and IV, the basis functions for center-fed and CPW-fed slot antennas are defined, by resorting to infinite delta-gap excited reference problems, respectively. The results are compared with those achieved using a fine meshing piecewise sinusoidal expansion. In Section V, the accuracy of the entire-domain basis functions analysis is also verified by comparison with measurements for the input impedance of a millimeter wave CPW-fed double-slot antenna. Conclusions are drawn in Section VI.

II. Formulation of the Problem

In this section, the magnetic-field integral equation is set up for some actual reference geometries.

A. Reference Geometries

The geometries of some typical slot antenna structures are shown in Fig. 1. A rectangular reference coordinate systems with the z axis orthogonal to the ground plane and the x axis parallel to the radiating slots is introduced. The unit vector of the coordinate axes are denoted by $\boldsymbol{i}_x, \boldsymbol{i}_y, \boldsymbol{i}_z$. All the apertures are etched on an infinite ground plane that separates two different homogeneous dielectrics (denoted by 1 and 2) with relative permittivity $\epsilon_{r1}, \epsilon_{r2}$. Fig. 1(a) shows a slot antenna fed by an impressed tangential component of the magnetic field concentrated at its center. This field is uniform in the region $x \in (-t/2,\ t/2)$, $y \in (-w_s/2,\ w_s/2)$ and zero elsewhere. The impressed magnetic fields will be denoted by $\boldsymbol{h}^{f1}(x, y)$ and $\boldsymbol{h}^{f2}(x, y)$ at the limit $z = 0^+$ and $z = 0^-$, respectively (see the inset). For all the configurations presented in Fig. 1 it will be assumed, $\boldsymbol{h}^{f1} = -\boldsymbol{h}^{f2} = \boldsymbol{h}^f/2$. The impressed field may be interpreted via the equivalence principle as impressed electric surface currents $\boldsymbol{j}^f/2 = \boldsymbol{i}_z \times \boldsymbol{h}^f/2$ which flow at $z = 0^+$ and $z = 0^-$ with the same amplitude and sign. These can also be seen as a unique strip of current $\boldsymbol{j}^f$ placed at $z = 0$ [see the insets to Fig. 1(a)]. The same criteria for the excitation are used for the two arrangements in Fig. 1(b) and (c), which presents models closer to practical configurations. In Fig. 1(b), the magnetic fields (electric currents) are impressed to feed a CPW which is connected to the slot. Fig. 1(c) presents a typical solution for the double slot, often used for millimeter-wave integrated antennas [3], [4] in connection with a bolometer. Again, the inset to these latter figures show the details of the feeding structure, with inclusion of the subdomain basis functions that will be discussed next.

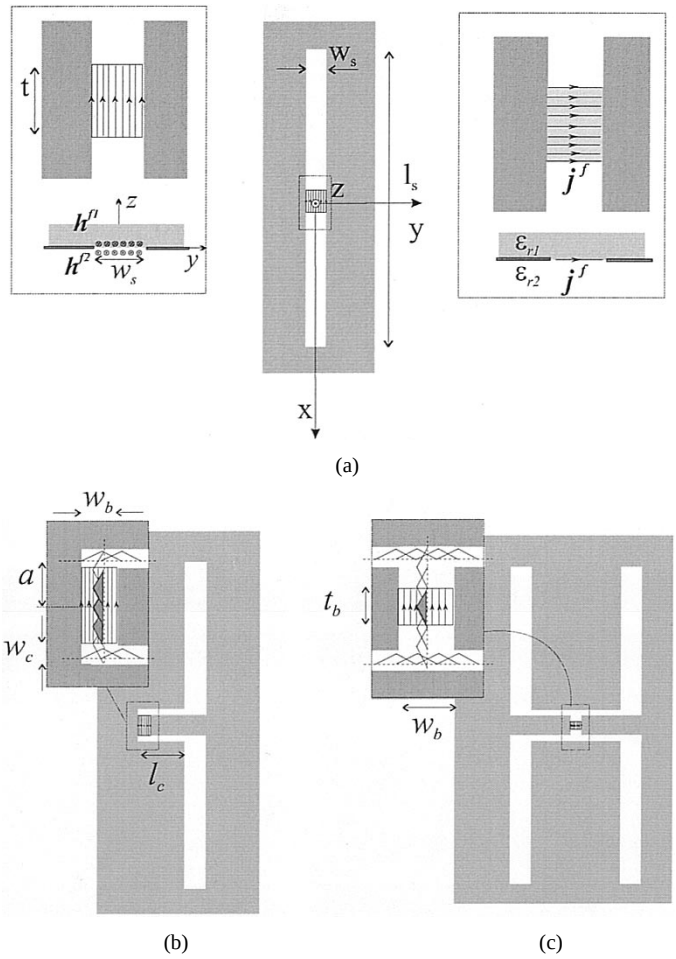

Fig. 1. Geometries of various slot antenna configurations. The slots are fed by an impressed magnetic field. The insets show the detail of the feed. (a) Centered feed slot [inset: (left) magnetic impressed field on the opposite parts of the slots and (right) interpretation in terms of an electric strip current]. (b) CPW-fed slot (inset: excitation of the CPW via magnetic impressed field and distribution of the subdomain basis functions). (c) Double-slot fed by two CPW branches in parallel (inset: symmetric magnetic field excitation which occupies a region smaller than the inner CPW conductor).

B. Integral Equation

Let us define Σ as the total region occupied by the apertures on the ground plane. By invoking the equivalence principle, the aperture regions are replaced by infinitely thin perfectly conducting plugs with two unknown magnetic current distributions $\pm\boldsymbol{m}(x',\ y')$ above and below the ground plane on Σ. These currents have equal amplitudes and opposite signs to ensure the continuity of the electric tangent field through the slots. An integral equation is formulated, which expresses the enforcement of the appropriate continuity through the apertures of the total (impressed plus radiated) magnetic field (CMFIE). All the magnetic currents radiate in a semi-infinite homogeneous medium which is bound by an infinite ground plane. According to the image principle one can reconstruct the field radiated in regions 1 and 2 by assuming a magnetic current of intensity $2\boldsymbol{m}$ and $-2\boldsymbol{m}$, respectively, radiating in a homogeneous infinite space. The CMFIE may be expressed by

$$\underline{\underline{\boldsymbol{g}}} * \boldsymbol{m} = -\boldsymbol{h}^f \tag{1}$$

where $*$ denotes the convolution product $\underline{\underline{\boldsymbol{g}}} = 2(\underline{\underline{\boldsymbol{g}}}_1 + \underline{\underline{\boldsymbol{g}}}_2)$ and $\underline{\underline{\boldsymbol{g}}}_i$ is the dyadic Green's function of the tangent magnetic field associated with a magnetic dipole radiating in the homogeneous medium i.

C. Fine Mesh MoM Solution and Matrix Compression

To solve (1) by the MoM, the magnetic current is approximated in terms of the small-domain basis function $\boldsymbol{b}_q$

$$\boldsymbol{m} \simeq \sum_{q=1}^{Q} V_q \boldsymbol{b}_q \tag{2}$$

that is assumed to be directed along the x axis on the radiating slots, and along the y axis on the CPW slots. In (2), V_q represents the unknown weights. The basis functions $\boldsymbol{b}_q$ are centered at the points (x_q, y_q) of the domain Σ. The overlapping of orthogonal functions in the corner region must be imposed in order to guarantee the continuity of the magnetic currents [see the insets to Fig. 1(b) and (c)]. The conventional Galerkin-MoM solution scheme can now be applied to (1) to determine the unknown expansion coefficients V_q. Testing both the left- and right-hand side of (1) onto the same functions $\boldsymbol{b}_q$ leads to the linear system

$$\sum_{q=1}^{Q} V_q Y_{qq'} = I_{q'}; \quad q' = 1 \ldots Q \tag{3}$$

where

$$Y_{qq'} = \langle \boldsymbol{b}_q, \boldsymbol{b}_{q'} * \underline{\underline{\boldsymbol{g}}} \rangle, \quad I_{q'} = \langle \boldsymbol{b}_{q'}, -\boldsymbol{h}^f \rangle \tag{4}$$

and the inner product $\langle \cdot, \cdot \rangle$ is the usual reaction-type integral extended to the aperture domain Σ. When few problem-matched entire-domain basis functions $\boldsymbol{m}_n$ are used to expand the unknowns

$$\boldsymbol{m} \simeq \sum_{n=1}^{N} v_n \boldsymbol{m}_n; \quad N \ll Q \tag{5}$$

the problem is converted into a small linear system

$$\sum_{n=1}^{N} v_n y_{nn'} = i_{n'}; \quad n' = 1, \ldots N \tag{6}$$

where

$$y_{nn'} = \langle \boldsymbol{m}_n, \boldsymbol{m}_{n'} * \underline{\underline{\boldsymbol{g}}} \rangle, \quad i_{n'} = \langle \boldsymbol{m}_{n'}, -\boldsymbol{h}^f \rangle. \tag{7}$$

To calculate the reaction integral in (7), a spectral-domain formulation may be appropriate. However, when a small-domain algorithm is already available, it can be convenient to see $y_{nn'}$ as originating from a compression of the original matrix $Y_{qq'}$. To achieve this, one can represent each entire-domain function $\boldsymbol{m}_n(x, y)$ in terms of $\boldsymbol{b}_q$ as

$$\boldsymbol{m}_n \simeq \sum_{q=1}^{Q} M_{nq} \boldsymbol{b}_q \tag{8}$$

where $\mathbf{M}_{nq}$ may be found by simply sampling $m_n(x, y)$ at (x_q, y_q). Applying (8) to (7) yields the compression relationship

$$y_{nn'} = \sum_{q=1}^{Q} \sum_{q'=1}^{Q} M_{nq} M_{n'q'} Y_{qq'}; \quad i_{n'} = \sum_{q'=1}^{Q} M_{n'q'} I_{q'}. \tag{9}$$

In the following sections, appropriate entire-domain basis functions are defined on the basis of the Green's function of infinite transmission line problems.

III. Center-Fed Slot

In this section, the entire-domain basis functions for the MoM analysis of the center-fed slot [Fig. 1(a)] are determined. It is useful to underline two aspects which provide the guidelines for the determination of the most appropriate set of basis functions to be used in this problem.

1) The resonant behavior of the slot can be described in terms of interference between traveling waves coming both from the center and from the slot endpoints. These traveling waves can be constructed on the basis of the exact propagation constant for an infinite slot-line. However, these traveling waves alone are not sufficient to describe the field excited in the proximity of the actual feed, and further source-attached basis functions are needed.
2) The source reactance strongly depends on the physical dimension of the feeding electric currents [$''t''$ in Fig. 1(a)], and is almost independent of the slot length. Accurate prediction of the resonant frequency depends on this reactance. Hence, source-attached functions must be used to model the source region.

A. Green's Function of an Infinite Slot-Line

An infinite slot-line is considered, with the same width w_s of the slot and etched on an infinite ground plane between the same two dielectric half-spaces (ϵ_{r1}, ϵ_{r2}). The slot line is excited by an elementary electric dipole $\boldsymbol{i}_y \delta(x) rect(y, w_s)$, where $rect(y, w_s)$ is unity in $y \in (-w_s/2, w_s/2)$ and zero elsewhere. The method for the analytical calculation of the Green's function of this problem is presented in [10] and [11]. The solution procedure assumes a separability between transverse and longitudinal space dependence of the field, which is commonly used for thin slots. This procedure, which is conceptually the same as that adopted in [13]–[15], is based on: 1) expanding via Fourier transform the impressed magnetic field in spectral superposition of longitudinal traveling waves with k_x wavenumber; 2) solving the two-dimensional CMFIE for each k_x, by a MoM scheme; and 3) integrating all the traveling-wave responses in k_x. In contrast with [13]–[15], in [10] and [11], the final representation is expressed in an explicit analytical form, thanks to the assumption of a given (but respecting edge-singularity) transverse dependence of the electric field and to a razor-blade testing on the slot axis of the two-dimensional integral equation. The Green's function for the electric field at $z = 0$ is finally obtained in spectral analytical form as

$$\boldsymbol{G}(x, y) = \frac{c \boldsymbol{i}_y}{\sqrt{1 - \left(\frac{2y}{w_s}\right)^2}} \int_{-\infty}^{\infty} \frac{e^{-jk_x x}}{D(k_x)} dk_x \tag{10}$$

where

$$D(k_x) = \sum_{i=1}^{2} \left(k_i^2 - k_x^2\right) J_0\left(\frac{w_s}{4}\sqrt{k_i^2 - k_x^2}\right) \times H_0^{(2)}\left(\frac{w_s}{4}\sqrt{k_i^2 - k_x^2}\right) \tag{11}$$

where $c = (4k_0\zeta_0/w_s\pi)$, and $H_0^{(2)}$ and J_0 are the Hankel function of the second kind and the Bessel function, respectively. In

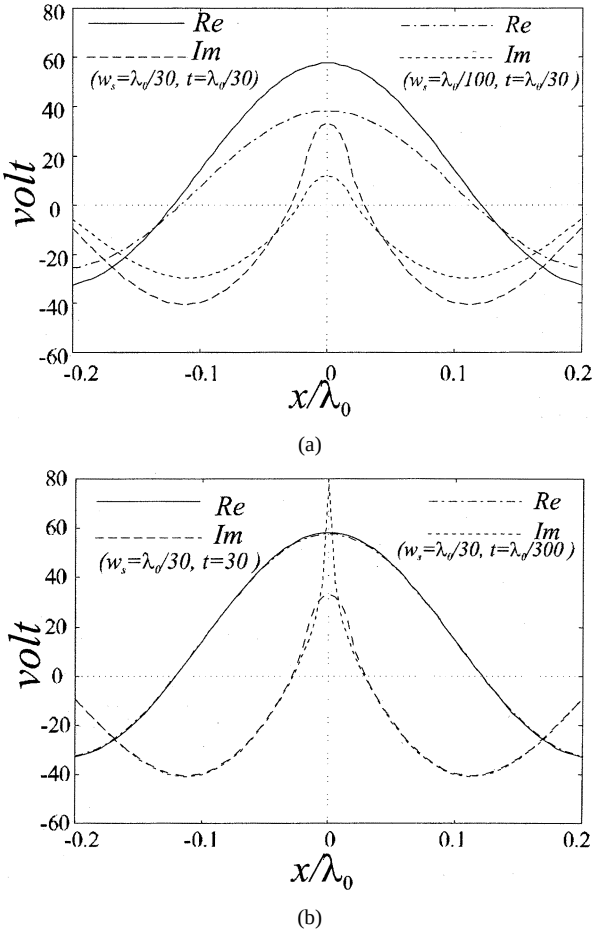

Fig. 2. Normalized electric-field distribution $(w_s \cdot \boldsymbol{E}(x, y = 0))$ as a function of the distance x from the center (in free-space wavelengths) for infinite slots between homogeneous silicon and free space (a) $w_s = \lambda_0/30$ and $w_s = \lambda_0/100$ with the same delta-gap $(t = \lambda_0/30)$ and (b) $t = \lambda_0/30$ and $t = \lambda_0/300$ with the same widths $(w_s = \lambda_0/30)$.

(10), the branches associated to the square roots in the integrand are such that $Im(\sqrt{k_i^2 - k_x^2}) < 0$ on the relevant top Riemann sheet, and the integration contour detours the branch points at $k_x = \pm k_i$ in counterclockwise and clockwise sense, respectively.

To obtain the slot-field for the excitation $\boldsymbol{j}^f = \boldsymbol{i_y}(I_0/t)rect(x,t)rect(y,w_s)$, one simply multiplies the integrand in (10) by the $\mathbf{k}_x$-spectrum of $rect(x,t)$, namely by $I_0 sinc(k_x t/2)$, thus obtaining the electric field

$$E(x,y) = \frac{I_0 c}{\sqrt{1-\left(\frac{2y}{w_s}\right)^2}} \int_{-\infty}^{\infty} \frac{sinc\left(\frac{k_x t}{2}\right) e^{-jk_x x}}{D(k_x)} dk_x. \quad (12)$$

Fig. 2 shows the real and the imaginary part of $E(x,y)$ for two values of w_s and t. The imaginary part $E(x,y)$ shows a peak in the vicinity of the source which is associated to the storage of local reactive energy. This peak tends to a logarithmic singularity as t tends to zero. The distribution of the real part of $E(x,y)$ presents a shape almost independent on the extension t of the delta gap. The dependence on the slot's width w_s is essentially the same in the real and imaginary parts.

B. Slot Resonant Mode

The infinite slot-line supports a leaky, quasi-TEM traveling mode. Its complex propagation constant can be found analytically by solving the dispersion equation $D(k_{x0}) = 0$. In [10] and [11], it is shown that for small values of w_s, the solution of $D(k_{x0}) = 0$ tends to the constant β

$$k_{x0} \to \beta = \sqrt{\frac{(k_1^2 + k_2^2)}{2}} \quad (13)$$

which is associated to the average of two permittivities, as one would expect. A couple of traveling waves are used to describe the resonant mode on the finite slot by interference. To achieve this, two symmetric basis functions are shaped as inward- and outward-propagating waves with respect to the center of the finite slot, and are defined as follows:

$$\boldsymbol{m}_{1,2}(x,y) = \frac{rect(x,l_s)rect(y,w_s)}{\sqrt{1-\left(\frac{2y}{w_s}\right)^2}} e^{\mp jk_{x0}|x|} \boldsymbol{i}_x \quad (14)$$

where the subscript 1 (2) refers to the upper (lower) sign. The two functions $\boldsymbol{m}_1$ and $\boldsymbol{m}_2$ are used as independent basis functions in the MoM formulation. Note that the attenuation of the leaky mode for practical values of w_s is so small that expression (13) for k_{x0} holds in most practical cases. If the slots are part of an array, also an asymmetric traveling-wave basis function, with the same propagation constant k_{x0} should be included to account for unbalancing due to external mutual coupling.

C. Source-Attached Mode

For large x in terms of the wavelength, the integral in (12) can be asymptotically evaluated by deforming the original contour into the steepest descent path, and including the residue $R(y)$ associated to the pole k_{x0} captured in this deformation. Thus, the total field $E(x,y)$ can be expressed as the sum of two contributions. The steepest descent path contribution represents the source-dependent field $E^s(x,y)$, and the residue contribution represents a couple of outgoing traveling waves. $E^s(x,y)$ will be used to form the source attached MoM basis functions. Accordingly, $E^s(x,y)$ can be expressed as

$$E^s(x,y) = E(x,y) - 2\pi j \frac{I_0 c\, sinc\left(\frac{k_{x0} t}{2}\right)}{\sqrt{1-\left(\frac{2y}{w_s}\right)^2}} R(y) e^{-jk_{x0}|x|} \quad (15)$$

where R(y) is the residue of $(D(k_x))^{-1}$ at k_{x0}. To actually account for the field in the vicinity of the feeding source in a MoM scheme, two basis functions shaped as the real and the imaginary part of $\boldsymbol{E}^s$ are defined on the domain of the finite slot as

$$\boldsymbol{m}_3(x,y) = \frac{1}{I_0 c} rect(x,l_s)rect(y,w_s) Re\left[E^s(x,y)\right] \boldsymbol{i}_x \quad (16)$$

$$\boldsymbol{m}_4(x,y) = \frac{1}{I_0 c} rect(x,l_s)rect(y,w_s) I_m\left[E^s(x,y)\right] \boldsymbol{i}_x. \quad (17)$$

The source-attached basis functions could have been defined directly from the total field $E(x,y)$ rather than $E^s(x,y)$. The definition adopted here is preferable because a separation between the resonant mode and the source-attached mode is achieved. When the width of the slot is small and the imaginary part of the propagation constant is not dominant, this choice

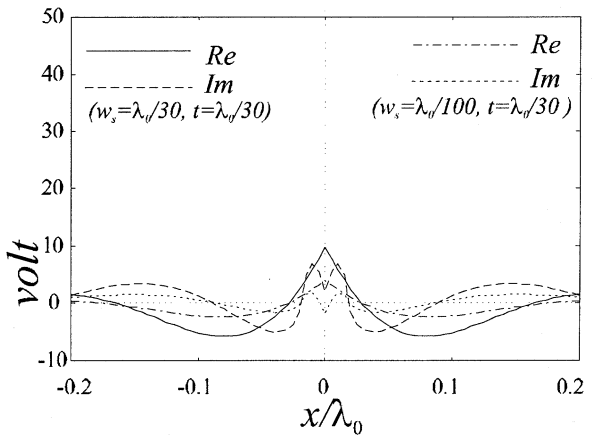

(a)

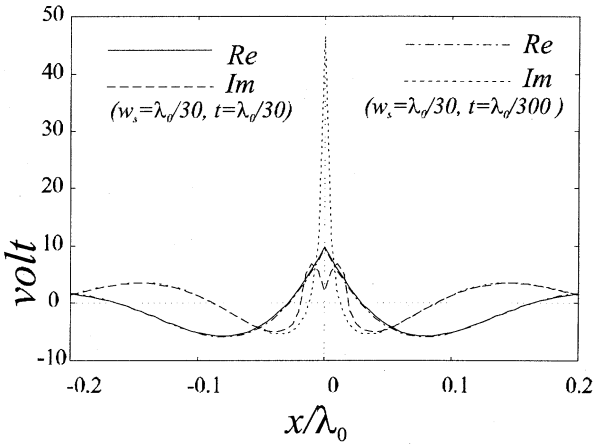

(b)

Fig. 3. Normalized source-attached electric-field distribution $(w \cdot \boldsymbol{E}^s(x, y = 0))$ as a function of the distance x from the center (in free space wavelength) for infinite slots between hogeneous silicon and free space (a) $w_s = \lambda_0/30$ and $w_s = \lambda_0/100$ with the same delta-gap $(t = \lambda_0/30)$ and (b) $t = \lambda_0/30$ and $t = \lambda_0/300$ with the same widths $(w_s = \lambda_0/30)$.

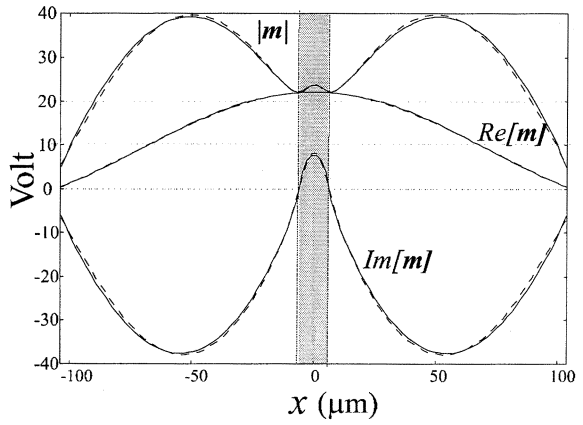

(a)

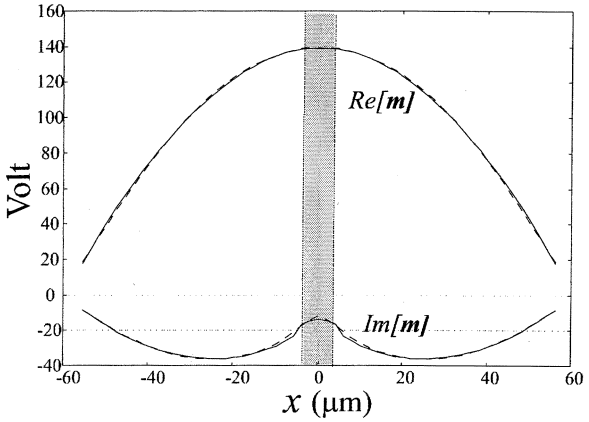

(b)

Fig. 4. The curves plot the product of the magnetic currents by w_s to obtain a voltage across the slot as a function of x for center-fed slots [Fig. 1(a)] with $t = 14\ \mu$m, $w_s = 10\ \mu$m, $f = 500$ GHz, $\epsilon_{r1} = 11.7$ (silicon), $\epsilon_{r2} = 1$. Continuous line: fine mesh MoM with PWS basis functions; dashed line: MoM with four entire-domain basis function. (a) Approximately one-wavelength slot ($l_s = 210\ \mu$m, $f = 500$GHz). (b) Approximately half-wavelength slot ($l_s = 116\ \mu$m, $f = 500$GHz). Note the compressed scale with respect to (a).

allows a faster decay $(x^{-3/2})$ moving away from the source [10]–[15]. Fig. 3 shows the real and the imaginary part of $E^s(x, y)$ for various values of w_s and t. The amplitude of $E^s(x, y)$ is smaller with respect to the amplitude of $E(x, y)$ (see Fig. 2 and note the different scale), which means that the total field is dominated by the travelling-wave (residue) contribution. Finally, it should be noted that while both real and imaginary parts of $E^s(x, y)$ increase with the slot's width (w_s), the delta-gap dimension (t) only affects the imaginary part of $E^s(x, y)$ in the source region. $Im[E^s]$ peaks near to $x = 0$, for $t = \lambda_0/300$ [see Fig. 3(b)].

D. Comparisons With Small-Domain MoM

In order to provide a reference solution for the structure in Fig. 1(a), a fine meshing MoM with piece wise sinusoidal basis functions has been implemented. To achieve convergence of the imaginary part of the slot impedance, at least three piecewise sinusoidal functions must be devoted to cover the zone over which the impressed field is distributed. This allows to adequately account for the inductance associated to the width t of the electric source and the corresponding accurate description of the resonant frequency. In a uniform-mesh MoM, this also dictates the number of basis functions to be used. The results are compared in Fig. 4 with those obtained from a MoM analysis with entire-domain basis functions as described in Section III-B and III-C. The lengths of the slots are $l_s = 210\ \mu$m and $l_s = 116\ \mu$m for Fig. 4(a) and (b), respectively. At the operating frequency of 500 GHz, these correspond approximately to the second and the first resonance, respectively (i.e., one and one half effective wavelengths, respectively). For both cases, the dielectric constants of the media are $\epsilon_{r1} = 11.7$ *(silicon)* and $\epsilon_{r2} = 1$, the slot widths are $w_s = 10\ \mu$m, and the strip-sources have $t = 14\ \mu$m [see Fig. 1(a)]. The curves represent the amplitude, real, and imaginary part of the voltage across the slot (i.e., magnetic currents multiplied by w_s) as a function of the coordinate x (expressed in μm). Excellent agreement has been found between results from the fine meshing MoM (41 and 21 basis functions for Fig. 4(a) and (b), respectively) and those from the MoM solution with four entire-domain basis functions. The input electric current I_0 is assumed to be unity so that the voltage level at $x = 0$ can be directly interpreted as the input impedance. It should be noted that the level of the impedance for the full-wavelength slot is much lower than the level of the half-wave-

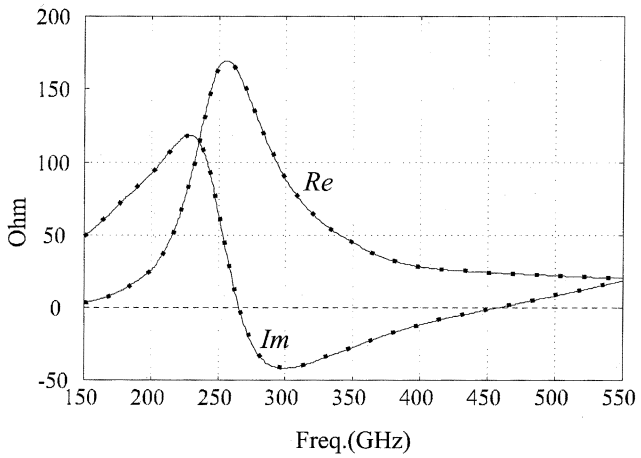

Fig. 5. Real (Re) and imaginary (Im) parts of the input impedance against the frequency for a center-fed slot [Fig. 1(a)] with $l_s = 210\ \mu$m, $t = 14\ \mu$m, $w_s = 10\ \mu$m, $\epsilon_{r1} = 11.7$ (silicon), $\epsilon_{r2} = 1$. Continuous line: fine mesh MoM with PWS basis functions. Dotted line: MoM with four entire-domain basis function.

length slot, so that the former may be more easily matched to the typical characteristic impedance of a CPW. When the slot length is gradually decreased in terms of a wavelength, the impact of traveling-wave modes becomes increasingly dominant. This means that the feed attachment modes could have been neglected. However, the combined use of source attached and traveling-wave modes allows the correct description of the magnetic current solution at all frequencies. In order to validate the entire-domain basis function MoM procedure over a large frequency range, the input impedance versus frequency is shown in Fig. 5. Real and imaginary parts of the impedance calculated with the present method are shown and compared to those from the fine meshing MoM analysis, and two nearly superimposed curves can be observed.

IV. CPW-Fed Slot

In the previous section, the entire-domain basis functions for the MoM analysis of the center-fed slot was determined. In this section the applicability of the entire-domain basis functions will be extended to incorporate the cases of Fig. 1(b) and (c). The CPW-fed slot antenna [Fig. 1(b)] constitutes a practical realization of the center-fed slot when assuming that the inner conductor of the CPW has the same width of the delta gap in the previous model. While still using the slot description presented previously, a refinement is described in this section to account for the presence of the CPW connection through 90° bends. The corresponding traveling-wave currents on the CPW are also introduced.

A. CPW Feed Description

As shown in Fig. 1(b), the CPW is fed by the same impressed electric current (magnetic field) as that used for the center-fed slot in Fig. 1(a). The impressed current is uniformly distributed in a region which may [Fig. 1(b)] or may not [Fig. 1(c)] occupy the entire inner conductor of the CPW. This model is believed to be more accurate with respect to models that define the excitation through a couple of voltage generators connecting the inner conductor of the CPW to the outer ground plane. The latter method requires a "black box" representation of the CPW feed-region. The present model adequately takes into account the reactive energy stored in the source vicinity. This is important especially when the physical space occupied by the physical device is smaller than the inner CPW conductor (see Fig. 1(c), which corresponds to a solution often used for bolometric receivers).

B. Traveling-Wave Currents in the CPW

To model the CPW, while maintaining the number of unknowns small in the MoM scheme, appropriate entire-domain basis functions are used that are shaped as the quasi-TEM traveling modes supported by the CPW. The magnetic currents associated to a forward traveling mode are then represented as

$$\boldsymbol{m}_5(x,y) = \boldsymbol{m}_u^+(x,y) + \boldsymbol{m}_l^+(x,y) \tag{18}$$

where the two contributions are relevant to the upper and lower arms of the CPW

$$\begin{aligned} \boldsymbol{m}_u^+(x,y) &= e^{-jk_{ycpw}y}\boldsymbol{i}_y; \quad y = (-\infty,\infty), \\ & \qquad x = \left(a - \frac{w_c}{2}, a + \frac{w_c}{2}\right) \\ \boldsymbol{m}_l^+(x,y) &= e^{-jk_{ycpw}y}\boldsymbol{i}_y; \quad y = (-\infty,\infty), \\ & \qquad x = \left(-a - \frac{w_c}{2}, -a + \frac{w_c}{2}\right). \end{aligned} \tag{19}$$

The y axis is placed at the center of the part lying between the two arms. A similar backward propagating basis function, indicated as $\boldsymbol{m}_6(x,y)$, is also defined on the same domain to account for the reflection. In (19), k_{ycpw} can be determined by solving the dispersion equation arising from the solution of the infinitely extended CPW problem. This latter has been investigated [12] using the same approach as that described in III-A for the infinite slot-line and the final dispersion equation is represented as

$$\int_{-\infty}^{\infty} G(k_x, k_{ycpw}) J_0\left(\frac{k_x w_c}{2}\right) sin^2(k_x a) dk_x = 0 \tag{20}$$

where J_0 is the Bessel function and

$$G(k_x,k_y) = \frac{-j}{k_0\zeta_0}\left(\frac{\left(\epsilon_{r1}k_0^2 - k_y^2\right)}{\sqrt{\epsilon_{r1}k_0^2 - k_x^2 - k_y^2}} - \frac{\left(\epsilon_{r2}k_0^2 - k_y^2\right)}{\sqrt{\epsilon_{r2}k_0^2 - k_x^2 - k_y^2}}\right) \tag{21}$$

is the spectrum of the pertinent Green's function. For all practical CPW dimensions k_{ycpw} can be approximated by $\beta = \sqrt{(k_1^2 + k_2^2)/2}$.

C. Distortion Due to the Bends

The CPWs are connected to either the slot [Fig. 1(b)] or the actual source [inset to Fig. 1(c)] through 90° bend junctions, which deserve special attention. To guarantee convergence of a

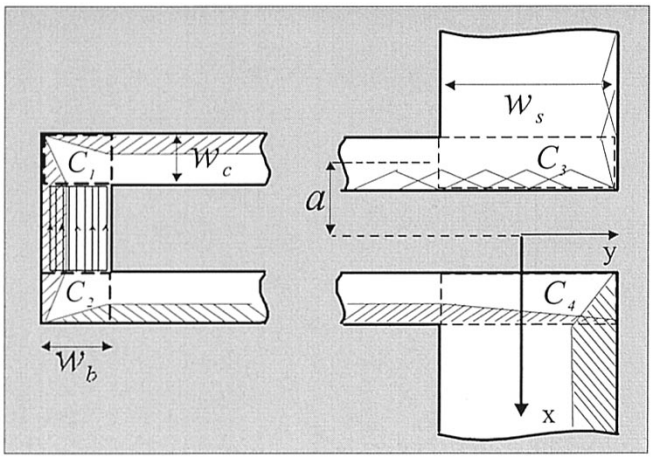

(a) (b)

Fig. 6. (a) CPW-feed connection and (b) CPW-slot connection. The bend windowing function that $W(\boldsymbol{r})$ is represented with provides a linear tapering of the traveling-wave basis functions thus ensuring respect of vanishing tangential field at the corner termination. The entire-domain basis functions defined in (8), (9) and (11), (12) are still used after multiplication for $W(\boldsymbol{r})$. In (a) one PWS function (dark) is used to cover the feed region. The PWS fine meshing is shown in the upper drawing of (b).

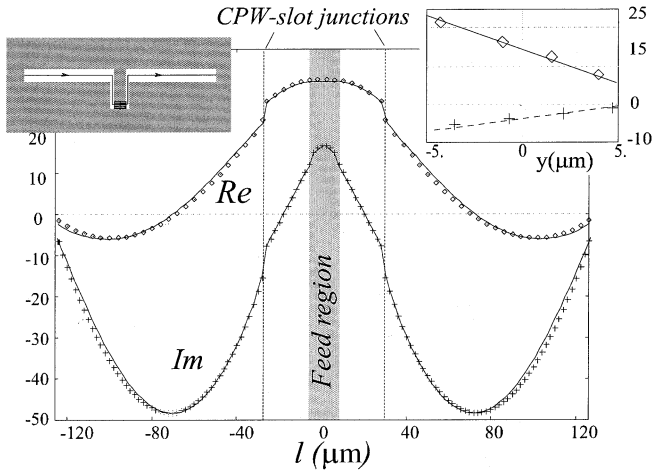

Fig. 7. The curves plot the product of the magnetic currents by w_s (voltage across the apertures) as a function of a linear coordinate l along the structure for centered CPW-fed slots [Fig. 1(b)] with $a = 6\ \mu$m, $w_s = 10\ \mu$m, $l_s = 210\ \mu$m, $l_c = 20\ \mu$m, $w_c = 2\mu$m, $f = 500$ GHz, $\epsilon_{r1} = 11.7$ (silicon), $\epsilon_{r2} = 1$. Continuous line: fine mesh MoM with PWS basis functions. Crosses and squares: MoM with entire-domain basis function (four modes).

small-domain planar waveguides (PWS) MoM for such a junction, a fine meshing must be used [9]. The x-directed electric field along the y-directed branch of the bend vanishes at the corner since it meets the x-directed metallic edge of the other branch of the bend [see Fig. 6(b)]. Numerical investigations carried out on a fine meshing MoM have shown that this field decays over a very small region of space. According to the entire-domain function description, it is proposed to include, directly in those basis functions, approximate information on the rapidly varying, vanishing field at the corners. This can be achieved by extending the region in which the basis functions are defined to include the corner regions, and tapering the field with a linear profile to zero. An expansion of the corner regions of Fig. 1(b) is depicted in Fig. 6. The rectangular domains defined inside the dashed lines of Fig. 6(a) and (b) are indicated by C_1, C_2, C_3, and C_4, while the difference domain $\Sigma - C_1 - C_2 - C_3 - C_4$, where Σ is the overall aperture domain, is denoted Δ. Then, a windowing function $W(x, y)$ with domain on Σ is defined that equals unity on Δ and linearly goes to zero in both the variables x and y in all the regions C_i [see the dashed regions in Fig. 6(a) and (b)]. To ensure a vanishing tangential field at each corner termination all the entire-domain basis functions defined in the previous sections are simply multiplied by $W(x, y)$. Using this concept it is possible to use the same entire-domain basis functions defined for the center-fed slot.

D. Numerical Examples and Physical Interpretation

The results presented in Fig. 7 are for a CPW-fed slot whose length and width are the same as in the case of Fig. 4(a). The geometrical dimensions of the CPW are $w_c = 2\ \mu$m, $a = 6\ \mu$m, and the length of the CPW line is $l_c = 20\ \mu$m (see Fig. 1). The entire-domain basis functions used in the overall analysis are the following.

1) Four x-oriented basis functions (Section III, $\boldsymbol{m}_1, \boldsymbol{m}_2, \boldsymbol{m}_3, \boldsymbol{m}_4$) used to model the center-fed slot, in which the parameter t has been set equal to the width of the CPW inner conductor ($t = 2a - w_c$).
2) Two y-oriented basis functions on the CPW arms in the form of an incident and a reflected wave, respectively (Section IV-B; $\boldsymbol{m}_5$, $\boldsymbol{m}_6$).
3) One constant basis function on the feed region defined as in Fig. 6(a) ($\boldsymbol{m}_7$).

These seven functions are linearly tapered to zero at the bends via multiplication by $W(x, y)$. The reference fine mesh solution uses 67 PWS functions (making use of symmetry). The results of the entire-domain MoM and the PWS MoM analysis are presented in Fig. 7. The voltages across the slot width (real and imaginary parts) are shown as a function of a linear coordinate, with origin at the center of the feed point. The agreement is excellent. The continuity of the magnetic currents is observed everywhere except at the connection between the CPW and the radiating slot. The inset zooms in on the details of this connection. A linear variation of both the real and the imaginary parts of the y-directed magnetic current is found and plotted as a function of y for $x = (a - w_c/2, a + w_c/2)$ (refer to the coordinate system drawn in Fig. 6(b) for corner C_4). The linear approximation described by $W(x, y)$ is validated by the fine meshing MoM solution. The storage of reactive energy in the bend is responsible for the voltage jump. The two 90° bends of the CPW-slot connection essentially behave as reactive lumped loads.

V. Double-Slot Antenna

The double-slot antenna in Fig. 1(c) has actually been breadboarded, within the framework of an European Space Agency contract [16]–[18], in the laboratories of the Space Research Organization Netherlands (SRON). The focusing towards the double slot itself of a broadside incoming plane wave is achieved via a silicon dielectric elliptical lens. The geometrical dimensions of the structure under analysis are $a = 25\ \mu m$, $w_c = 10\ \mu m$, $I_c = 247.5\ \mu m$, $w_s = 50\ \mu m$, $l_s = 1050\ \mu m$ and $w_b =$

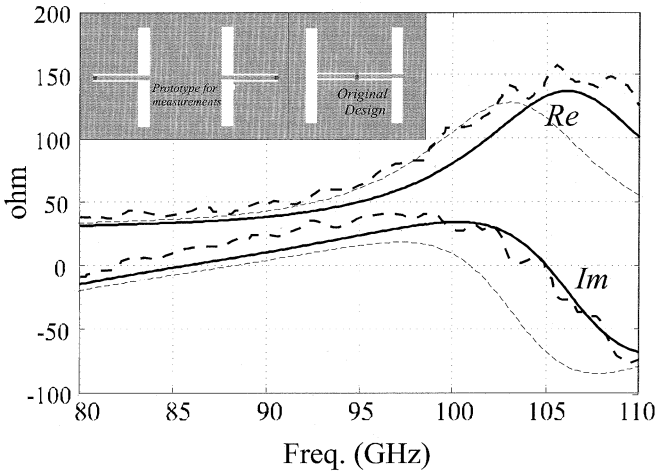

Fig. 8. Real (Re) and imaginary(Im) parts of the input impedance against the frequency for a double-slot antenna-fed slot with $a = 25\ \mu m$, $w_c = 10\ \mu$m, $l_c = 247.5\ \mu$m, $w_s = 50\ \mu$m, $l_s = 1050\ \mu$m, $w_b = 10\ \mu$m, $\epsilon_{r1} = 11.7$ (silicon), $\epsilon_{r2} = 1$. Prototype antenna: MoM with entire-domain basis functions (continuous line); measurements (large dashed line). Design antenna: MoM with entire-domain basis functions (fine dashed line).

$10\ \mu m$; the investigated range of frequency is 80–110 GHz. The diameter of the elliptical lens is 20 mm. The slot antenna which has been designed for the receiver is like that of Fig. 1(c). However, in order to facilitate impedance measurements at those frequencies, a prototype has been realized, where the slots are fed by CPWs printed on the opposite sides with respect to the center ([16], see the inset of Fig. 8). The measurements of the S-parameters have been carried out at the two port prototype by a network analyzer, and, from the S-data, an equivalent input impedance has been derived for the original one port H-type design. The measured data is represented by the thick dashed line. The numerical results (continuous line) agree well with those from the measurements. The third curve (dashed thin line) corresponds to the numerical simulation of the H-type design, fed at the center. It is worth noting that this latter result deviates slightly from the others due to the CPW-CPW interactions occurring in the H-type geometry. In the frame of this work, the impact of the reflections inside the lens due to the silicon-air interface has been neglected, and in the present analysis the upper and lower half spaces are assumed to be infinite homogeneous silicon and free space, respectively.

As presented in [16]–[18], the oscillations observed in the measurements are due to these reflections. It has been shown in [18], by means of a physical optics approach, that the impact on the input impedance of elements close to the focus is mainly oscillatory as a function of frequency.

VI. Conclusion

A method has been presented to accurately model CPW-fed slot antenna by means of Green's function-based entire-domain MoM basis functions. These entire-domain basis functions on the resonant slot are based on the analytical solution for a gap-excited infinite slot-line. These basis functions include attachment modes associated to the source and traveling modes which reconstruct the resonant mode on the slot. Furthermore, traveling waves based on a quasi-analytical solution of the infinitely extended CPW problem, are used to describe the stationary field in the finite CPWs. The CPW-slot transition, 90° bends, are described by linearly tapering the profile of the entire-domain basis functions to zero at the corners.

Since each of the geometrical dimensions of the structures is a parameter in a specific basis function, the numerical analysis is independent from these dimensions, so that the method is particularly suitable for a parametric investigations to aid the design. Overall, the procedure is very well suited for accurate design purposes, considering the excellent agreement with results achieved via a fine grid MoM implementation and its numerical efficiency.

Acknowledgment

The double-slot antenna has been manufactured by the Space Research Organization (SRON), The Netherlands. The relevant input impedance measurements have been performed by the University of Glasgow (Scotland, U.K.).

References

[1] D. B. Rutledge, D. P. Neikirk, and D. P. Kasilingam, "Integrated circuit antennas," in *Infrared and Millimeter Waves*, K. J. Button, Ed. New York: Academic, 1983, vol. 10, pp. 1–90.

[2] G. M. Rebeiz, "Millimeter wave and terahertz integrated circuit antennas," *Proc. IEEE*, vol. 80, pp. 1748–1770, Nov. 1992.

[3] M. J. M. van der Vorst, P. J. I. de Maagt, and M. H. A. Herben, "Effect of internal reflections on the radiation properties and input admittance of integrated lens antennas," *IEEE Trans. Microwave Theory Tech.*, vol. 47, pp. 1696–1704, Sept. 1999.

[4] M. Van der Vorst, P. J. I. de Maagt, A. Neto, A. Reynolds, W. Luinge, R. Heres, and M. Herben, "Effect of the internal reflections on the radiation properties and input impedance of integrated lens antennas: comparison between theory and measurements," *IEEE Trans. Microwave Theory Tech.*, vol. 49, pp. 1118–1125, June 2001.

[5] T. M. Weller, L. P. B. Katehi, and G. M. Rebeiz, "Single and double folded antennas on semi-infinite substrates," *IEEE Trans. Antennas Propagat.*, vol. 43, pp. 1423–1428, Dec. 1995.

[6] P. Otero, G. V. Eleftheriades, and J. Mosig, "Integrated modified rectangular loop slot antenna on substrate lenses for mm and sub-mm wave frequencies mixer applications," *IEEE Trans. Antennas Propagat.*, vol. 46, Oct. 1998.

[7] D. M. Pozar, "A reciprocity method of analysis for printed slot and slot-coupled microstrip antennas," *IEEE Trans. Antennas Propagat.*, vol. 34, pp. 1439–1446, 1986.

[8] J. Laheurte, L. Katehi, and G. M. Rebeiz, "CPW fed slot antennas on multilayer dielectric substrates," *IEEE Trans. Antennas Propagat.*, vol. 44, pp. 1102–1111, Aug. 1996.

[9] T. F. Huang, S. W. Lu, and P. Hsu, "Analysis and design of coplanar waveguide fed slot antenna array," *IEEE Trans. Antennas Propagat.*, vol. 47, pp. 1560–1565, Oct. 1999.

[10] A. Neto and S. Maci, "Green's function of an infinite slot printed between two homogeneous dielectrics. Part I: magnetic currents," Jet Propulsion Laboratory Internal Rep. (D/21 321), Pasadena, CA, 2001.

[11] A. Neto and S. Maci, "Green's function of an infinite slot printed between two homogeneous dielectrics. Part I: magnetic currents," *IEEE Trans. Antennas Propagat.*, vol. 51, p. xref, June 2003.

[12] D. Pasqualini, A. Neto, and R. Wyss, "Distributed sources in coplanar waveguides: Application to phototmixer based THz local oscillators," *Microwave Opt. Technol. Lett.*, vol. 33, no. 6, June 2002.

[13] C. Di Nallo, F. Mesa, and D. R. Jackson, "Excitation of leaky modes on multilayer stripline structures," *IEEE Trans. Microwave Theory Tech.*, vol. 46, pp. 1062–1071, Aug. 1998.

[14] F. Mesa, C. Di Nallo, and D. R. Jackson, "The theory of surface-wave and space-wave leaky-mode excitation on microstrip lines," *IEEE Trans. Microwave Theory Tech.*, vol. 47, pp. 207–215, Feb. 1999.

[15] D. R. Jackson, F. Mesa, C. Di Nallo, and D. P. Nyquist, "The theory of surface-wave and space-wave leaky-mode excitation on microstrip lines," *Radio Sci.*, vol. 35, pp. 495–510, Mar.-Apr. 2000.

[16] I. G. Thayne, D. L. Edgar, K. Elgaid, H. McLelland, S. Ferguson, A. Ross, J. M. Arnold, R. M. Heeres, N. Whyborn, W. Luinge, M. J. M. van der Vorst, A. Neto, and P. J. I. de Maagt, "On wafer determination of impedance of planar 100 GHz double slot antenna," *Electron. Lett.*, vol. 35, no. 16, pp. 1291–1292, Aug. 1999.

[17] A. Neto, S. Maci, and P. J. I. de Maagt, "Reflections inside an elliptical dielectric lens antenna," *Proc. Inst. Elect. Eng. Microwaves, Antennas, Propagat.*, vol. 145, no. 3, pp. 243–247, June 1998.

[18] A. Neto, L. Borselli, S. Maci, and P. J. I. de Maagt, "Input impedance of integrated elliptical dielectric lens antennas," *Proc. Inst. Elect. Eng. Microwaves, Antennas, Propagat.*, vol. 146, no. 3, pp. 181–186, June 1999.

Andrea Neto (M'99) was born in Naples, Italy, in 1968. He received the M.S. degree (with honors) in electronic engineering from the University of Florence, Italy, in 1994 and the Ph.D. degree in methods for the analysis of large arrays from the University of Siena, Italy, in 1999.

Part of his studies were developed at the European Space Agency Research and Technology Center, Noordwijk, the Netherlands, where he worked in the Antenna Section. From 2000 to 2001, he was a Postdoctoral Researcher at the California Institute of Technology, Pasadena. In particular, he was working for the Sub-mm Wave Advanced Technology Group, Jet Propulsion Laboratory, Pasadena. Currently, he is with the Physics and Electronics Laboratory, TNO, Den Haag, the Netherlands. His research is focused on analytical and numerical methods in electromagnetics.

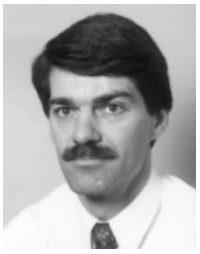

Peter De Maagt (S'88–M'88–SM'02) was born in Pauluspolder, The Netherlands, in 1964. He received the M.Sc. and Ph.D. degrees from Eindhoven University of Technology, Eindhoven, The Netherlands, in 1988 and 1992, respectively, both in electrical engineering.

He is currently with the European Space Research and Technology Centre (ESTEC), European Space Agency, Noordwijk, The Netherlands. His research interests are in the area of millimeter and submillimeter-wave reflector and planar integrated antennas, quasi-optics, photonic bandgap antennas, and millimeter-and submillimeter-wave components.

Dr. De Maagt was a co-recipient of the H. A. Wheeler award of the IEEE Antennas and Propagation Society for the best applications paper of 2001 and a recipient of a 2002 ESA Award for innovation.

Stefano Maci (M'92–SM'99) was born in Rome, Italy, in 1961. He received the Ph.D. degree in electronic engineering from the University of Florence, Florence, Italy, in 1987.

From 1990 to 1998, he was with the Department of Electronic Engineering, University of Florence, as an Assistant Professor. In 1998, he was appointed Associate Professor of Electromagnetism at the University of Siena, Siena, Italy. During 1997, he was an invited Professor at the Technical University of Denmark, Copenhagen. His research interests are focused on electromagnetic theory, mainly concerning high- and low-frequency methods for antennas and electromagnetic scattering. Since 1996, he has been responsible for the University of Siena's projects with the European Space Agency and with other european industries. He is principal author or coauthor of approximately 60 articles in international journals and more than 150 papers in proceedings of international conferences.

Dr. Maci was an Associate Editor of IEEE TRANSACTIONS ON ELECTROMAGNETIC COMPATIBILITY from 1998 to 2001. He received the National Young Scientists "Francini" Award for his Laurea thesis in 1987 and the "Barzilai" Prize for the best paper at the National Italian Congress of Electromagnetism (XI RiNEm) in 1996.